

## Research Paper

# Analysis of Delamination in Two-Dimensional Functionally Graded Multilayered Beam with Non-Linear Behaviour of Material

Victor Iliev RIZOV

*Department of Technical Mechanics  
University of Architecture, Civil Engineering and Geodesy  
1 Chr. Smirnensky blvd., 1046 – Sofia, Bulgaria  
e-mail: v\_rizov\_fhe@uacg.bg*

An analytical study of delamination fracture in a two-dimensional functionally graded multilayered beam exhibiting material non-linearity is carried-out. The beam is made of adhesively bonded horizontal layers. The material is two-dimensional functionally graded in the cross-section of each layer. A delamination crack is located symmetrically with respect to the beam mid-span. The delamination is studied in terms of the strain energy release rate. The solution derived is compared with the  $J$ -integral for verification. The effects of material gradients, the crack location along the beam height and the material non-linearity on the delamination fracture are investigated. The distribution of the  $J$ -integral value along the crack front is analysed too.

**Key words:** two-dimensional functionally graded material; multilayered beam; delamination; material non-linearity; analytical solution.

## 1. INTRODUCTION

Functionally graded materials are inhomogeneous composites made by mixing of two different constituent materials. A desired continuous variation of microstructure and mechanical properties in one or more directions is generated during manufacturing of functionally graded materials, so as to provide benefits of both of constituent materials [1]. The composition of functionally graded materials can be tailored in order to obtain a predetermined composition profile. Therefore, these novel materials are applied mainly in the development of structural members and components subjected to non-uniform service requirements. Fracture mechanics plays a basic role in assessing of integrity and safety of structural members and components made of functionally graded materials.

Therefore, fracture behaviour of these materials continues to attract the attention of researchers [2–5].

Works dealing with fracture behaviour of functionally graded materials have been reviewed in [2]. Various analyses of cracks oriented both parallel and perpendicular to the material gradient direction have been summarized. In these analyses, methods of linear-elastic fracture mechanics have been applied. Fracture studies under static or fatigue crack loading conditions have been considered. Various solutions for rectilinear cracks, circular arc cracks and slightly curved cracks have been presented.

Cracks in functionally graded beams under three-point bending have been analysed assuming linear-elastic behaviour of the material in [3]. The compliance approach for evaluation of fracture has been explored. An equivalent homogeneous beam of variable height has been suggested. It has been found that the compliance of the cracked functionally graded beam is well approximated by an equivalent homogeneous beam with cubic variation of height. It has been shown that the equivalent compliance concept is particularly suitable to gain insight regarding the mechanics of cracks in functionally graded structural components loaded by concentrated forces.

Free vibration problems of cracked functionally graded beams have been analysed in [4]. It has been assumed that the modulus of elasticity varies along the beam height (i.e., the material is one dimensional functionally graded). Both clamped-clamped and clamped-free beam configurations have been investigated. The fracture analysis has been performed assuming that the beam, which has a transversal crack, can be modelled as two sub-beams connected by a rotational spring of zero mass. The effects of crack location and crack depth on the dynamic fracture behaviour have been discussed.

Longitudinal fracture in a functionally graded cantilever beam configuration has been analysed with taking into account the non-linear behaviour of the material in [5]. It has been assumed that the material is one dimensional functionally graded. A vertical crack located arbitrary along the width of the beam cross-section has been investigated.

Multilayered systems, manufactured by bonding of layers of different materials, are characterized by high strength to weight and stiffness to weight ratios. Therefore, these systems are very suitable for structural applications, where low weight is an important issue. Delamination, i.e. fracture along interfaces between layers, is a type of failure often seen in multilayered structures. Therefore, significant efforts have been devoted to investigate the delamination phenomenon in multilayered materials [6–8].

Delamination fracture in multilayered functionally graded non-linear elastic beams has been studied in [6]. It has been assumed that the material is one dimensional functionally graded in each layer. A solution to the strain energy



taking into account the non-linear behaviour of the material. The beam is made of an arbitrary number of horizontal layers. Perfect adhesion is assumed between layers. A vertical notch of depth,  $h_2$ , is introduced in the beam mid-span in order to generate conditions for delamination fracture. A delamination crack of length,  $2a$ , is located symmetrically with respect to the beam mid-span. The thicknesses of the lower and upper crack arms are  $h_1$  and  $h_2$ , respectively. The beam cross-section is a rectangle of width,  $b$ , and height,  $2h$ . The beam is loaded by two bending moments of magnitude,  $M$ , applied in the free ends of the beam as shown in Fig. 1. It is obvious that the upper crack arms are free of stresses.

Due to the symmetry, only half of the beam,  $l \leq x_3 \leq 2l$ , is analysed. The strain energy release rate,  $G$ , in non-linear elastic beams can be written as [5]

$$(2.1) \quad G = \frac{dU^*}{b da},$$

where  $dU^*$  is the change of the complementary strain energy,  $da$  is an elementary increase of the crack length.

The present analysis is valid for non-linear elastic behaviour of material. The analysis can also be used for elastic-plastic behaviour of material if the beam undergoes active deformation, i.e. if the external loading increases only [9]. It should also be noted that the present analysis is based on the small strains assumption.

In order to determine  $G$  by formula (2.1), the complementary strain energy,  $U^*$ , has to be expressed as a function of the delamination crack length,  $a$ . For this purpose, the complementary strain energy density is integrated in the lower crack arm,  $l \leq x_3 \leq l + a$ , and the un-cracked beam portion,  $l + a \leq x_3 \leq 2l$ :

$$(2.2) \quad U^* = a \sum_{i=1}^{i=n_L} \int_{z_{1i}}^{z_{1i+1}} \left( \int_{-(b/2)}^{b/2} u_{0L_i}^* dy_1 \right) dz_1 \\ + (l - a) \sum_{1=i}^{i=n} \int_{z_{2i}}^{z_{2i+1}} \left( \int_{-(b/2)}^{b/2} u_{0U_i}^* dy_2 \right) dz_2,$$

where  $u_{0L_i}^*$  and  $u_{0U_i}^*$  are the complementary strain energy densities in the  $i$ -th layer of the lower crack arm and un-cracked beam portion, respectively. Axes,  $y_1$  and  $z_1$ , and coordinates,  $z_{1i}$  and  $z_{1i+1}$ , are shown in Fig. 2,  $y_2$  and  $z_2$  are the centroidal axes of the cross-section of un-cracked beam portion ( $z_2$  is directed downwards). In Eq. (2.2),  $n_L$  and  $n$  are the numbers of layers in the lower crack arm and the un-cracked beam portion, respectively.

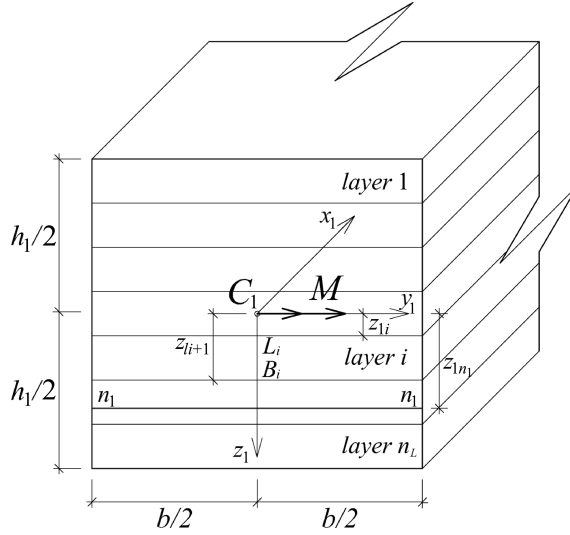


FIG. 2. The geometry and loading of the lower crack arm cross-section in the beam mid-span (the neutral axis position is marked by  $n_1-n_1$ ).

The material behaviour in the  $i$ -th layer of the beam is described by the following power-law stress-strain relation [10]:

$$(2.3) \quad \sigma_i = S_i \varepsilon^{m_i},$$

where  $S_i$  and  $m_i$  are material properties in the same layer. The material is two-dimensional functionally graded in the cross-section of each layer. Thus, the material property,  $S_i$ , varies continuously in the cross-section of the  $i$ -th layer according to the following law:

$$(2.4) \quad S_i = S_{H_i} \frac{64y_1^6}{b^6} + \frac{S_{B_i} - S_{L_i}}{(z_{1i+1} - z_{1i})^3} (z_1 - z_{1i})^3 + S_{L_i},$$

where

$$(2.5) \quad -\frac{b}{2} \leq y_1 \leq \frac{b}{2}, \quad z_{1i} \leq z_1 \leq z_{1i+1}.$$

In Eq. (2.4),  $S_{H_i}$  is a material property that governs the material gradient along the width of the layer,  $S_{B_i}$  and  $S_{L_i}$  are the values of  $S_i$  in points  $B_i$  and  $L_i$ , respectively (Fig. 2).

Formula (2.4) shows that the material property,  $S_i$ , is distributed symmetrically with respect to vertical axis,  $z_1$ .

In principle, the complementary strain energy density is equal to the area  $OQR$  that supplements the area  $OPQ$ , enclosed by the stress-strain curve, to

a rectangle (Fig. 3). The complementary strain energy density in the  $i$ -th layer of lower crack arm, when the material behaviour is described by the power-law stress-strain relation, can be expressed as [6]

$$(2.6) \quad u_{0L_i}^* = S_i \frac{m_i \varepsilon^{m_i+1}}{m_i + 1}.$$

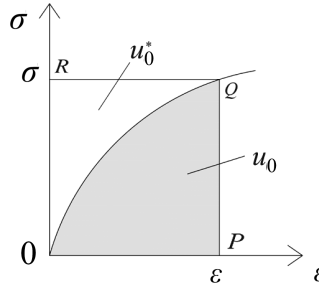


FIG. 3. Non-linear stress-strain curve ( $u_0$  and  $u_0^*$  are the strain energy and the complementary strain energy densities, respectively).

The strain energy density is equal to the area  $OPQ$ , enclosed by the stress-strain curve (Fig. 3). The strain energy density in the  $i$ -th layer of lower crack arm can be written as [6]

$$(2.7) \quad u_{0L_i} = \frac{S_i \varepsilon^{m_i+1}}{m_i + 1}.$$

The Bernoulli's hypothesis for plane sections is used to analyse the distribution of strains since the span to height ratio of the beam under consideration is large. Concerning application of the Bernoulli's hypothesis in the present analysis, it should also be noted that since the beam is loaded in pure bending (Fig. 1) the only non-zero strain is the longitudinal strain,  $\varepsilon$ . Therefore, according to the small strain compatibility equations,  $\varepsilon$  is distributed linearly along the height of the beam cross-section. Thus,  $\varepsilon$  in the lower crack arm (Fig. 2) is written as

$$(2.8) \quad \varepsilon = (z_1 - z_{1n_1}) \kappa_1,$$

where  $z_{1n_1}$  is the coordinate of the neutral axis,  $\kappa_1$  is the curvature of the lower crack arm. It should be noted that the neutral axis,  $n_1-n_1$ , shifts from the centroid since the beam is multilayered and functionally graded (Fig. 2).

By substituting of (2.4) and (2.8) in (2.6), one obtains

$$(2.9) \quad u_{0L_i}^* = \left[ S_{H_i} \frac{64y_1^6}{b^6} + \frac{S_{B_i} - S_{L_i}}{(z_{1i+1} - z_{1i})^3} (z_1 - z_{1i})^3 + S_{L_i} \right] \cdot \frac{m_i (z_1 - z_{1n_1})^{m_i+1} \kappa_1^{m_i+1}}{m_i + 1}.$$

Formula (2.9) describes the distribution of the complementary strain energy density in the cross-section of the  $i$ -th layer of the lower crack arm.

The quantities,  $z_{1n_1}$  and  $\kappa_1$ , which participate in (2.9) are determined from the following equilibrium equations of lower crack arm cross-section:

$$(2.10) \quad N_1 = \sum_{i=1}^{i=n_L} \int_{z_{1i}}^{z_{1i+1}} \left( \int_{-(b/2)}^{b/2} \sigma \, dy_1 \right) dz_1,$$

$$(2.11) \quad M_{y_1} = \sum_{i=1}^{i=n_L} \int_{z_{1i}}^{z_{1i+1}} \left( \int_{-(b/2)}^{b/2} \sigma z_1 \, dy_1 \right) dz_1,$$

where  $N_1$  and  $M_{y_1}$  are the axial force and bending moment, respectively. It can be observed in Fig. 2 that

$$(2.12) \quad N_1 = 0, \quad M_{y_1} = M.$$

By substituting of (2.3), (2.4) and (2.8) in (2.10) and (2.11), the equilibrium equations take the form

$$(2.13) \quad N_1 = \sum_{i=1}^{i=n_L} \left\{ \left[ \frac{S_{L_i} b \kappa_1^{m_i}}{m_i + 1} + \frac{S_{H_i} b \kappa_1^{m_i}}{7(m_i + 1)} + \frac{\lambda_i b \kappa_1^{m_i} (-z_{1i})^3}{m_i + 1} \right] (\rho_i^{m_i+1} - v_i^{m_i+1}) \right. \\ + 3\lambda_i b \kappa_1^{m_i} z_{1i}^2 \left[ \frac{1}{m_i + 2} (\rho_i^{m_i+2} - v_i^{m_i+2}) + \frac{z_{1n_1}}{m_i + 1} (\rho_i^{m_i+1} - v_i^{m_i+1}) \right] \\ - 3\lambda_i b \kappa_1^{m_i} z_{1i} q_i \left[ \frac{1}{f_i + 3q_i} \left( \rho_i^{\frac{f_i+3q_i}{q_i}} - v_i^{\frac{f_i+3q_i}{q_i}} \right) + \frac{2z_{1n_1}}{f_i + 2q_i} \left( \rho_i^{\frac{f_i+2q_i}{q_i}} - v_i^{\frac{f_i+2q_i}{q_i}} \right) \right. \\ \left. \left. + \frac{z_{1n_1}^2}{f_i + q_i} \left( \rho_i^{\frac{f_i+q_i}{q_i}} - v_i^{\frac{f_i+q_i}{q_i}} \right) \right] \right. \\ \left. + \lambda_i b \kappa_1^{m_i} q_i \left[ \frac{1}{f_i + 4q_i} \left( \rho_i^{\frac{f_i+4q_i}{q_i}} - v_i^{\frac{f_i+4q_i}{q_i}} \right) + \frac{3z_{1n_1}}{f_i + 3q_i} \left( \rho_i^{\frac{f_i+3q_i}{q_i}} - v_i^{\frac{f_i+3q_i}{q_i}} \right) \right. \right. \\ \left. \left. + \frac{3z_{1n_1}^2}{f_i + 2q_i} \left( \rho_i^{\frac{f_i+2q_i}{q_i}} - v_i^{\frac{f_i+2q_i}{q_i}} \right) + \frac{z_{1n_1}^3}{f_i + q_i} \left( \rho_i^{\frac{f_i+q_i}{q_i}} - v_i^{\frac{f_i+q_i}{q_i}} \right) \right] \right\},$$

$$\begin{aligned}
(2.14) \quad M_{y_1} = & \sum_{i=1}^{i=n_L} \left\{ \left[ S_{L_i} \kappa_1^{m_i} b + \frac{S_{H_i} \kappa_1^{m_i} b}{7} + \lambda_i \kappa_1^{m_i} b (-z_{1i})^3 \right] \right. \\
& \times \left[ \frac{1}{m_i + 2} \left( \rho_i^{m_i+2} - v_i^{m_i+2} \right) + \frac{z_{1n_1}}{m_i + 1} \left( \rho_i^{m_i+1} - v_i^{m_i+1} \right) \right] \\
& + 3\lambda_i \kappa_1^{m_i} b z_{1i}^2 q_i \left[ \frac{1}{f_i + 3q_i} \left( \rho_i^{\frac{f_i+3q_i}{q_i}} - v_i^{\frac{f_i+3q_i}{q_i}} \right) + \frac{2z_{1n_1}}{f_i + 2q_i} \left( \rho_i^{\frac{f_i+2q_i}{q_i}} - v_i^{\frac{f_i+2q_i}{q_i}} \right) \right. \\
& \left. \left. + \frac{z_{1n_1}^2}{f_i + q_i} \left( \rho_i^{\frac{f_i+q_i}{q_i}} - v_i^{\frac{f_i+q_i}{q_i}} \right) \right] \right. \\
& - 3\lambda_i \kappa_1^{m_i} b z_{1i} q_i \left[ \frac{1}{f_i + 4q_i} \left( \rho_i^{\frac{f_i+4q_i}{q_i}} - v_i^{\frac{f_i+4q_i}{q_i}} \right) + \frac{3z_{1n_1}}{f_i + 3q_i} \left( \rho_i^{\frac{f_i+3q_i}{q_i}} - v_i^{\frac{f_i+3q_i}{q_i}} \right) \right. \\
& \left. + \frac{3z_{1n_1}^2}{f_i + 2q_i} \left( \rho_i^{\frac{f_i+2q_i}{q_i}} - v_i^{\frac{f_i+2q_i}{q_i}} \right) + \frac{z_{1n_1}^3}{f_i + q_i} \left( \rho_i^{\frac{f_i+q_i}{q_i}} - v_i^{\frac{f_i+q_i}{q_i}} \right) \right] \\
& + \lambda_i \kappa_1^{m_i} b q_i \left[ \frac{\rho_i^{f_i+5q_i} - v_i^{f_i+5q_i}}{f_i + 5q_i} + \frac{4z_{1n_1} \left( \rho_i^{f_i+4q_i} - v_i^{f_i+4q_i} \right)}{f_i + 4q_i} \right. \\
& \left. + \frac{6z_{1n_1}^2 \left( \rho_i^{f_i+3q_i} - v_i^{f_i+3q_i} \right)}{f_i + 3q_i} + \frac{4z_{1n_1}^3 \left( \rho_i^{f_i+2q_i} - v_i^{f_i+2q_i} \right)}{f_i + 2q_i} \right. \\
& \left. \left. + \frac{z_{1n_1}^4 \left( \rho_i^{f_i+q_i} - v_i^{f_i+q_i} \right)}{f_i + q_i} \right] \right\},
\end{aligned}$$

where  $\lambda_i = (S_{B_i} - S_{L_i}) / (z_{1i+1} - z_{1i})^3$ ,  $\rho_i = z_{1i+1} - z_{1n_1}$ ,  $v_i = z_{1i} - z_{1n_1}$  and  $f_i/q_i = m_i$  ( $f_i$  and  $q_i$  are positive integers).

Obviously, at  $m_i = 1$  the power-law stress-strain relation (2.3) transforms into the Hooke's law. This means that at  $m_i = 1$  formula (2.14) should yield the curvature of linear-elastic beam. Indeed, by substituting of  $m_i = 1$ ,  $n_L = 1$ ,  $S_{L_i} = S_{B_i} = E$  (here  $E$  is the modulus of elasticity) and  $S_{H_i} = 0$  in (2.14), one derives

$$(2.15) \quad \kappa_{z_1} = \frac{12M}{Ebh_1^3},$$

which is exact match of the expression for curvature of a linear-elastic homogeneous beam of width,  $b$ , and height,  $h_1$ .

Equations (2.13) and (2.14) should be solved with respect to  $z_{1n_1}$  and  $\kappa_1$  by using the MatLab computer program.

Formula (2.9) can also be applied to determine the distribution of the complementary strain energy density,  $u_{0U_i}^*$ , in the cross-section of the  $i$ -th layer of the un-cracked beam portion. For this purpose,  $y_1, z_1, z_{1i}, z_{1i+1}, z_{1n_1}$  and  $\kappa_1$  have to be replaced with  $y_2, z_2, z_{2i}, z_{2i+1}, z_{2n_2}$  and  $\kappa_2$ , respectively ( $z_{2n_2}$  and  $\kappa_2$  are the neutral axis coordinate and the curvature of the un-cracked beam portion, respectively). Equilibrium Eqs. (2.13) and (2.14) can be used to determine  $z_{2n_2}$  and  $\kappa_2$ . For this purpose,  $n_L, \lambda_i, \rho_i, v_i, z_{1i}, z_{1i+1}, z_{1n_1}$  and  $\kappa_1$  have to be replaced with  $n, \lambda_{U_i}, \rho_{U_i}, v_{U_i}, z_{2i}, z_{2i+1}, z_{2n_2}$  and  $\kappa_2$ , respectively. The quantities,  $\lambda_{U_i}, \rho_{U_i}, v_{U_i}$ , are written as  $\lambda_{U_i} = (S_{B_i} - S_{L_i}) / (z_{2i+1} - z_{2i})^3$ ,  $\rho_{U_i} = z_{2i+1} - z_{2n_2}$ ,  $v_{U_i} = z_{2i} - z_{2n_2}$ .

By substituting of  $u_{0L_i}^*, u_{0U_i}^*$  and Eq. (2.2) in (2.1) and doubling the expression obtained because of the symmetry (Fig. 1), one derives:

(2.16)

$$\begin{aligned}
 G = 2 \sum_{i=1}^{i=n_L} \frac{m_i \kappa_1^{m_i+1}}{b(m_i+1)} & \left\{ \left[ \frac{S_{L_i} b}{m_{t_i} + 1} + \frac{S_{H_i} b}{7(m_{t_i} + 1)} + \frac{\lambda_i b (-z_{1i})^3}{m_{t_i} + 1} \right] \left( \rho_i^{m_{t_i}+1} - v_i^{m_{t_i}+1} \right) \right. \\
 & + 3\lambda_i b z_{1i}^2 \left[ \frac{1}{m_{t_i} + 2} \left( \rho_i^{m_{t_i}+2} - v_i^{m_{t_i}+2} \right) + \frac{z_{1n_1}}{m_{t_i} + 1} \left( \rho_i^{m_{t_i}+1} - v_i^{m_{t_i}+1} \right) \right] \\
 & - 3\lambda_i b z_{1i} q_{t_i} \left[ \frac{1}{f_{t_i} + 3q_{t_i}} \left( \rho_i^{\frac{f_{t_i}+3q_{t_i}}{q_{t_i}}} - v_i^{\frac{f_{t_i}+3q_{t_i}}{q_{t_i}}} \right) + \frac{2z_{1n_1}}{f_{t_i} + 2q_{t_i}} \left( \rho_i^{\frac{f_{t_i}+2q_{t_i}}{q_{t_i}}} - v_i^{\frac{f_{t_i}+2q_{t_i}}{q_{t_i}}} \right) \right. \\
 & \left. \left. + \frac{z_{1n_1}^2}{f_{t_i} + q_{t_i}} \left( \rho_i^{\frac{f_{t_i}+q_{t_i}}{q_{t_i}}} - v_i^{\frac{f_{t_i}+q_{t_i}}{q_{t_i}}} \right) \right] \right. \\
 & + \lambda_i b q_{t_i} \left[ \frac{1}{f_{t_i} + 4q_{t_i}} \left( \rho_i^{\frac{f_{t_i}+4q_{t_i}}{q_{t_i}}} - v_i^{\frac{f_{t_i}+4q_{t_i}}{q_{t_i}}} \right) + \frac{3z_{1n_1}}{f_{t_i} + 3q_{t_i}} \left( \rho_i^{\frac{f_{t_i}+3q_{t_i}}{q_{t_i}}} - v_i^{\frac{f_{t_i}+3q_{t_i}}{q_{t_i}}} \right) \right. \\
 & \left. \left. + \frac{3z_{1n_1}^2}{f_{t_i} + 2q_{t_i}} \left( \rho_i^{\frac{f_{t_i}+2q_{t_i}}{q_{t_i}}} - v_i^{\frac{f_{t_i}+2q_{t_i}}{q_{t_i}}} \right) + \frac{z_{1n_1}^3}{f_{t_i} + q_{t_i}} \left( \rho_i^{\frac{f_{t_i}+q_{t_i}}{q_{t_i}}} - v_i^{\frac{f_{t_i}+q_{t_i}}{q_{t_i}}} \right) \right] \right\} \\
 - 2 \sum_{i=1}^{i=n} \frac{m_i \kappa_2^{m_i+1}}{b(m_i+1)} & \left\{ \left[ \frac{S_{L_i} b}{m_{t_i} + 1} + \frac{S_{H_i} b}{7(m_{t_i} + 1)} + \frac{\lambda_{U_i} b (-z_{2i})^3}{m_{t_i} + 1} \right] \left( \rho_{U_i}^{m_{t_i}+1} - v_{U_i}^{m_{t_i}+1} \right) \right. \\
 & + 3\lambda_{U_i} b z_{2i}^2 \left[ \frac{1}{m_{t_i} + 2} \left( \rho_{U_i}^{m_{t_i}+2} - v_{U_i}^{m_{t_i}+2} \right) + \frac{z_{2n_2}}{m_{t_i} + 1} \left( \rho_{U_i}^{m_{t_i}+1} - v_{U_i}^{m_{t_i}+1} \right) \right]
 \end{aligned}$$

(2.16)

[Cont.]

$$\begin{aligned}
& -3\lambda_{U_i} b z_{2i} q_{t_i} \left[ \frac{1}{f_{t_i} + 3q_{t_i}} \left( \frac{f_{t_i} + 3q_{t_i}}{\rho_{U_i}^{q_{t_i}}} - \nu_{U_i} \frac{f_{t_i} + 3q_{t_i}}{q_{t_i}} \right) + \frac{2z_{2n_2}}{f_{t_i} + 2q_{t_i}} \left( \frac{f_{t_i} + 2q_{t_i}}{\rho_{U_i}^{q_{t_i}}} - \nu_{U_i} \frac{f_{t_i} + 2q_{t_i}}{q_{t_i}} \right) \right. \\
& \qquad \qquad \qquad \left. + \frac{z_{2n_2}^2}{f_{t_i} + q_{t_i}} \left( \frac{f_{t_i} + q_{t_i}}{\rho_{U_i}^{q_{t_i}}} - \nu_{U_i} \frac{f_{t_i} + q_{t_i}}{q_{t_i}} \right) \right] \\
& + \lambda_{U_i} b q_{t_i} \left[ \frac{1}{f_{t_i} + 4q_{t_i}} \left( \frac{f_{t_i} + 4q_{t_i}}{\rho_{U_i}^{q_{t_i}}} - \nu_{U_i} \frac{f_{t_i} + 4q_{t_i}}{q_{t_i}} \right) + \frac{3z_{2n_2}}{f_{t_i} + 3q_{t_i}} \left( \frac{f_{t_i} + 3q_{t_i}}{\rho_{U_i}^{q_{t_i}}} - \nu_{U_i} \frac{f_{t_i} + 3q_{t_i}}{q_{t_i}} \right) \right. \\
& \qquad \qquad \qquad \left. + \frac{3y_{2n_2}^2}{f_{t_i} + 2q_{t_i}} \left( \frac{f_{t_i} + 2q_{t_i}}{\psi_{U_i}^{q_{t_i}}} - \zeta_{U_i} \frac{f_{t_i} + 2q_{t_i}}{q_{t_i}} \right) + \frac{y_{2n_2}^3}{f_{t_i} + q_{t_i}} \left( \frac{f_{t_i} + q_{t_i}}{\psi_{U_i}^{q_{t_i}}} - \zeta_{U_i} \frac{f_{t_i} + q_{t_i}}{q_{t_i}} \right) \right] \Bigg\}.
\end{aligned}$$

In formula (2.16),  $m_{t_i} = m_i + 1$ ,  $f_{t_i}/q_{t_i} = m_{t_i}$ , where  $f_{t_i}$  and  $q_{t_i}$  are positive integers.

Formula (2.16) expresses the strain energy release rate in the two-dimensional functionally graded multilayered beam configuration shown in Fig. 1, when the mechanical behaviour and the material gradient are described by formulae (2.3) and (2.4), respectively.

It should be noted that at  $m_i = 1$ ,  $n_L = 1$ ,  $n = 1$ ,  $h_1 = h_2 = h$ ,  $S_{L_i} = S_{B_i} = E$  and  $S_{H_i} = 0$  formula (2.16) yields

$$(2.17) \quad G = \frac{21M^2}{2Eb^2h^3},$$

which matches exactly the expression for the strain energy release rate when the beam is linear-elastic and homogeneous and the delamination crack is located in the beam mid-plane [11].

Formula (2.16) is verified by analysing the delamination crack with the help of the  $J$ -integral [12]. Due to the symmetry, only half of the beam is considered. The integration is carried-out by using an integration contour,  $\Gamma$ , that coincides with the beam contour (Fig. 1). It is obvious that the  $J$ -integral value is non-zero only in segments,  $\Gamma_1$  and  $\Gamma_2$ , of the integration contour ( $\Gamma_1$  and  $\Gamma_2$  coincide with the cross-section of the lower crack arm in the beam mid-span and the beam free end, respectively). Thus, the solution of the  $J$ -integral is written as

$$(2.18) \quad J = 2(J_{\Gamma_1} + J_{\Gamma_2}),$$

where  $J_{\Gamma_1}$  and  $J_{\Gamma_2}$  are the  $J$ -integral values in segments  $\Gamma_1$  and  $\Gamma_2$ , respectively. It should be noted that the expression in brackets in (2.18) is doubled because of the symmetry (Fig. 1).

The  $J$ -integral in segment,  $\Gamma_1$ , of the integration contour is written as

$$(2.19) \quad J_{\Gamma_1} = \sum_{i=1}^{n_L} \int_{z_{1i}}^{z_{1i+1}} \left[ u_{0L_i} \cos \alpha - \left( p_{xi} \frac{\partial u}{\partial x} + p_{yi} \frac{\partial v}{\partial x} \right) \right] ds,$$

where  $\alpha$  is the angle between the outwards normal vector to the contour of integration and the crack direction,  $p_{xi}$  and  $p_{yi}$  are the components of stress vector in the  $i$ -th layer of the lower crack arm,  $u$  and  $v$  are the components of displacement vector with respect to the crack tip coordinate system  $xy$  ( $x$  is directed along the crack),  $ds$  is a differential element along the contour.

The components of the  $J$ -integral in segment,  $\Gamma_1$ , are written as

$$(2.20) \quad p_{xi} = -\sigma_i = -S_i \varepsilon^{m_i}, \quad p_{yi} = 0,$$

$$(2.21) \quad ds = dz_1, \quad \cos \alpha = -1,$$

where coordinate,  $z_1$ , varies in the interval  $[-h_1/2, h_1/2]$ .

Formula (2.7) is applied to determine the strain energy density,  $u_{0L_i}$ . The following formula from mechanics of materials is applied to obtain the partial derivative,  $\partial u / \partial x$ , in (2.19):

$$(2.22) \quad \frac{\partial u}{\partial x} = \varepsilon = (z_1 - z_{1n_1}) \kappa_1,$$

where  $z_{1n_1}$  and  $\kappa_1$  are determined from equilibrium Eqs. (2.13) and (2.14).

By substituting of (2.3), (2.4), (2.7), (2.8), (2.20), (2.21) and (2.22) in (2.19), one derives

$$(2.23) \quad J_{\Gamma_1} = \sum_{i=1}^{i=n_L} \frac{m_i \kappa_1^{m_i+1}}{m_i + 1} \left\{ \left[ \frac{S_{L_i}}{m_{t_i} + 1} + \frac{64 S_{H_i} y_1^6}{b^6 (m_{t_i} + 1)} + \frac{\lambda_i (-z_{1i})^3}{m_{t_i} + 1} \right] \left( \rho_i^{m_{t_i}+1} - v_i^{m_{t_i}+1} \right) \right. \\ + 3 \lambda_i z_{1i}^2 \left[ \frac{1}{m_{t_i} + 2} \left( \rho_i^{m_{t_i}+2} - v_i^{m_{t_i}+2} \right) + \frac{z_{1n_1}}{m_{t_i} + 1} \left( \rho_i^{m_{t_i}+1} - v_i^{m_{t_i}+1} \right) \right] \\ - 3 \lambda_i z_{1i} q_{t_i} \left[ \frac{1}{f_{t_i} + 3q_{t_i}} \left( \rho_i^{\frac{f_{t_i}+3q_{t_i}}{q_{t_i}}} - v_i^{\frac{f_{t_i}+3q_{t_i}}{q_{t_i}}} \right) + \frac{2z_{1n_1}}{f_{t_i} + 2q_{t_i}} \left( \rho_i^{\frac{f_{t_i}+2q_{t_i}}{q_{t_i}}} - v_i^{\frac{f_{t_i}+2q_{t_i}}{q_{t_i}}} \right) \right. \\ \left. \left. + \frac{z_{1n_1}^2}{f_{t_i} + q_{t_i}} \left( \rho_i^{\frac{f_{t_i}+q_{t_i}}{q_{t_i}}} - v_i^{\frac{f_{t_i}+q_{t_i}}{q_{t_i}}} \right) \right] \right. \\ \left. + \lambda_i q_{t_i} \left[ \frac{1}{f_{t_i} + 4q_{t_i}} \left( \rho_i^{\frac{f_{t_i}+4q_{t_i}}{q_{t_i}}} - v_i^{\frac{f_{t_i}+4q_{t_i}}{q_{t_i}}} \right) + \frac{3z_{1n_1}}{f_{t_i} + 3q_{t_i}} \left( \rho_i^{\frac{f_{t_i}+3q_{t_i}}{q_{t_i}}} - v_i^{\frac{f_{t_i}+3q_{t_i}}{q_{t_i}}} \right) \right. \right. \\ \left. \left. + \frac{3z_{1n_1}^2}{f_{t_i} + 2q_{t_i}} \left( \rho_i^{\frac{f_{t_i}+2q_{t_i}}{q_{t_i}}} - v_i^{\frac{f_{t_i}+2q_{t_i}}{q_{t_i}}} \right) + \frac{z_{1n_1}^3}{f_{t_i} + q_{t_i}} \left( \rho_i^{\frac{f_{t_i}+q_{t_i}}{q_{t_i}}} - v_i^{\frac{f_{t_i}+q_{t_i}}{q_{t_i}}} \right) \right] \right\}.$$

It should be mentioned that in (2.23) the coordinate,  $y_1$ , varies in the interval  $[-b/2, b/2]$ .

Formula (2.23) can also be used to obtain the solution of the  $J$ -integral in segment,  $\Gamma_2$ , of the integration contour (Fig. 1). For this purpose,  $n_L$ ,  $\lambda_i$ ,  $\rho_i$ ,  $v_i$ ,  $z_{1i}$ ,  $z_{1i+1}$ ,  $z_{1n_1}$  and  $\kappa_1$  have to be replaced with  $n$ ,  $\lambda_{U_i}$ ,  $\rho_{U_i}$ ,  $v_{U_i}$ ,  $z_{2i}$ ,  $z_{2i+1}$ ,  $z_{2n_2}$  and  $\kappa_2$ , respectively. Also, the sign of Eq. (2.23) must be set to “minus” because the integration contour is directed upwards in segment,  $\Gamma_2$ .

By substituting of  $J_{\Gamma_1}$  and  $J_{\Gamma_2}$  in (2.18), one arrives at

(2.24)

$$\begin{aligned}
J = & 2 \sum_{i=1}^{i=n_L} \frac{m_i \kappa_1^{m_i+1}}{m_i+1} \left\{ \left[ \frac{S_{L_i}}{m_{t_i}+1} + \frac{64 S_{H_i} y_1^6}{b^6 (m_{t_i}+1)} + \frac{\lambda_i (-z_{1i})^3}{m_{t_i}+1} \right] \left( \rho_i^{m_{t_i}+1} - v_i^{m_{t_i}+1} \right) \right. \\
& + 3 \lambda_i z_{1i}^2 \left[ \frac{1}{m_{t_i}+2} \left( \rho_i^{m_{t_i}+2} - v_i^{m_{t_i}+2} \right) + \frac{z_{1n_1}}{m_{t_i}+1} \left( \rho_i^{m_{t_i}+1} - v_i^{m_{t_i}+1} \right) \right] \\
& - 3 \lambda_i z_{1i} q_{t_i} \left[ \frac{1}{f_{t_i}+3q_{t_i}} \left( \rho_i^{\frac{f_{t_i}+3q_{t_i}}{q_{t_i}}} - v_i^{\frac{f_{t_i}+3q_{t_i}}{q_{t_i}}} \right) + \frac{2z_{1n_1}}{f_{t_i}+2q_{t_i}} \left( \rho_i^{\frac{f_{t_i}+2q_{t_i}}{q_{t_i}}} - v_i^{\frac{f_{t_i}+2q_{t_i}}{q_{t_i}}} \right) \right. \\
& \left. \left. + \frac{z_{1n_1}^2}{f_{t_i}+q_{t_i}} \left( \rho_i^{\frac{f_{t_i}+q_{t_i}}{q_{t_i}}} - v_i^{\frac{f_{t_i}+q_{t_i}}{q_{t_i}}} \right) \right] \right. \\
& + \lambda_i q_{t_i} \left[ \frac{1}{f_{t_i}+4q_{t_i}} \left( \rho_i^{\frac{f_{t_i}+4q_{t_i}}{q_{t_i}}} - v_i^{\frac{f_{t_i}+4q_{t_i}}{q_{t_i}}} \right) + \frac{3z_{1n_1}}{f_{t_i}+3q_{t_i}} \left( \rho_i^{\frac{f_{t_i}+3q_{t_i}}{q_{t_i}}} - v_i^{\frac{f_{t_i}+3q_{t_i}}{q_{t_i}}} \right) \right. \\
& \left. \left. + \frac{3z_{1n_1}^2}{f_{t_i}+2q_{t_i}} \left( \rho_i^{\frac{f_{t_i}+2q_{t_i}}{q_{t_i}}} - v_i^{\frac{f_{t_i}+2q_{t_i}}{q_{t_i}}} \right) + \frac{z_{1n_1}^3}{f_{t_i}+q_{t_i}} \left( \rho_i^{\frac{f_{t_i}+q_{t_i}}{q_{t_i}}} - v_i^{\frac{f_{t_i}+q_{t_i}}{q_{t_i}}} \right) \right] \right\} \\
& - 2 \sum_{i=1}^{i=n} \frac{m_i \kappa_2^{m_i+1}}{m_i+1} \left\{ \left[ \frac{S_{L_i}}{m_{t_i}+1} + \frac{64 S_{H_i} y_1^6}{b^6 (m_{t_i}+1)} + \frac{\lambda_{U_i} (-z_{2i})^3}{m_{t_i}+1} \right] \left( \rho_{U_i}^{m_{t_i}+1} - v_{U_i}^{m_{t_i}+1} \right) \right. \\
& + 3 \lambda_{U_i} z_{2i}^2 \left[ \frac{1}{m_{t_i}+2} \left( \rho_{U_i}^{m_{t_i}+2} - v_{U_i}^{m_{t_i}+2} \right) + \frac{z_{2n_2}}{m_{t_i}+1} \left( \rho_{U_i}^{m_{t_i}+1} - v_{U_i}^{m_{t_i}+1} \right) \right] \\
& - 3 \lambda_{U_i} z_{2i} q_{t_i} \left[ \frac{1}{f_{t_i}+3q_{t_i}} \left( \rho_{U_i}^{\frac{f_{t_i}+3q_{t_i}}{q_{t_i}}} - v_{U_i}^{\frac{f_{t_i}+3q_{t_i}}{q_{t_i}}} \right) + \frac{2z_{2n_2}}{f_{t_i}+2q_{t_i}} \left( \rho_{U_i}^{\frac{f_{t_i}+2q_{t_i}}{q_{t_i}}} - v_{U_i}^{\frac{f_{t_i}+2q_{t_i}}{q_{t_i}}} \right) \right. \\
& \left. \left. + \frac{z_{2n_2}^2}{f_{t_i}+q_{t_i}} \left( \rho_{U_i}^{\frac{f_{t_i}+q_{t_i}}{q_{t_i}}} - v_{U_i}^{\frac{f_{t_i}+q_{t_i}}{q_{t_i}}} \right) \right] \right. \\
& + \lambda_{U_i} q_{t_i} \left[ \frac{1}{f_{t_i}+4q_{t_i}} \left( \rho_{U_i}^{\frac{f_{t_i}+4q_{t_i}}{q_{t_i}}} - v_{U_i}^{\frac{f_{t_i}+4q_{t_i}}{q_{t_i}}} \right) + \frac{3z_{2n_2}}{f_{t_i}+3q_{t_i}} \left( \rho_{U_i}^{\frac{f_{t_i}+3q_{t_i}}{q_{t_i}}} - v_{U_i}^{\frac{f_{t_i}+3q_{t_i}}{q_{t_i}}} \right) \right. \\
& \left. \left. + \frac{3y_{2n_2}^2}{f_{t_i}+2q_{t_i}} \left( \psi_{U_i}^{\frac{f_{t_i}+2q_{t_i}}{q_{t_i}}} - \zeta_{U_i}^{\frac{f_{t_i}+2q_{t_i}}{q_{t_i}}} \right) + \frac{y_{2n_2}^3}{f_{t_i}+q_{t_i}} \left( \psi_{U_i}^{\frac{f_{t_i}+q_{t_i}}{q_{t_i}}} - \zeta_{U_i}^{\frac{f_{t_i}+q_{t_i}}{q_{t_i}}} \right) \right] \right\}.
\end{aligned}$$

It should be noted that formula (2.24) expresses the distribution of the  $J$ -integral value along the delamination crack front. The average value of the  $J$ -integral along the delamination crack front is written as

$$(2.25) \quad J_{AV} = \frac{1}{b} \int_{-(b/2)}^{b/2} J dy_1.$$

The fact that the solution of the  $J$ -integral derived by substituting of (2.24) in (2.25) is exact match of the expression for the strain energy release rate (2.16) is a verification of the fracture analysis developed in the present paper.

### 3. NUMERICAL RESULTS

The influences of material gradient and crack location along the height of the beam cross-section on the delamination fracture behaviour are analysed. For this purpose, calculations of the strain energy release rate are carried-out by applying formula (2.16). In order to elucidate the effect of crack location along the height of the beam cross-section on the strain energy release rate, two three-layered beam configurations are analysed (Fig. 4). A delamination crack is located between layers 2 and 3 in the beam shown in Fig. 4a. A beam configuration with a crack between layers 1 and 2 is also investigated (Fig. 4b). Each layer in the beams in Fig. 4 has a thickness of  $t_l = 0.002$  m. The strain energy release rate is presented in non-dimensional form by using the formula  $G_N = G / (S_{L_3} b)$ . It is assumed that  $b = 0.020$  m,  $h = 0.003$  m,  $M = 30$  N·m,  $m_i = 0.7$ ,  $f_i = 7$ ,  $q_i = 10$ ,  $m_{t_i} = 1.7$ ,  $f_{t_i} = 17$  and  $q_{t_i} = 10$ , where  $i = 1, 2, 3$ . The material gradient along the width of layer 3 is characterized by  $S_{H_3}/S_{L_3}$  ratio. It should be specified that  $S_{L_3}$  is kept constant in the calculations. Therefore,  $S_{H_3}$  is varied in order to generate various  $S_{H_3}/S_{L_3}$  ratios. It is assumed that  $S_{L_1}/S_{L_3} = 1.2$ ,  $S_{H_1}/S_{L_1} = 1.4$ ,  $S_{B_1}/S_{L_1} = 1.3$ ,  $S_{L_2}/S_{L_3} = 1.5$ ,  $S_{H_2}/S_{L_2} = 1.1$ ,  $S_{B_2}/S_{L_2} = 1.2$  and  $S_{B_3}/S_{L_3} = 0.6$ . The strain energy release rate in non-dimensional form is presented as a function of  $S_{H_3}/S_{L_3}$  ratio in Fig. 5 for the two three-layered beam configurations shown in Fig. 4. It can be observed in Fig. 5 that the strain energy release rate decreases with increasing of  $S_{H_3}/S_{L_3}$  ratio (this is due to the increase of the beam stiffness). Figure 5 shows also the strain energy release rate decreases when the crack location is changed from this shown in Fig. 4a to that in Fig. 4b. This finding is attributed to the increase of the lower crack arm stiffness.

The effect of the material gradient along the thickness of layer 3 on the delamination fracture is evaluated too. The beam configuration shown in Fig. 4a is considered. The material gradient along the thickness of layer 3 is characterized by  $S_{B_3}/S_{L_3}$  ratio. The strain energy release rate in non-dimensional form

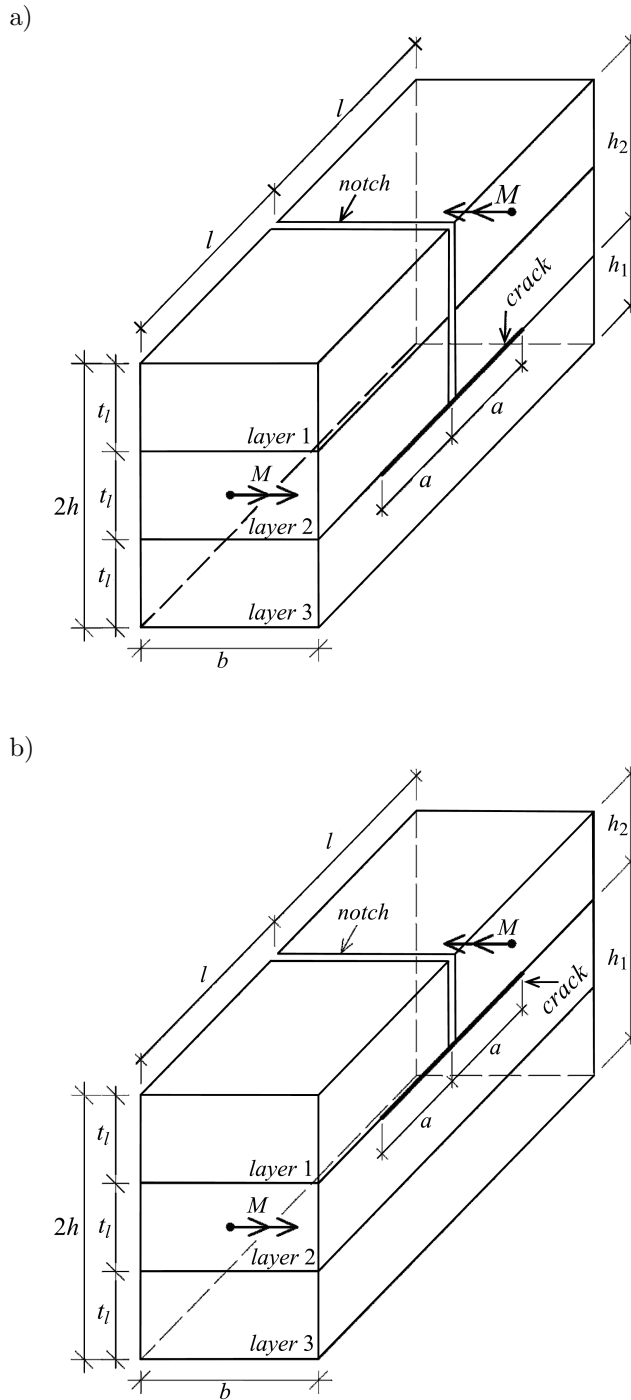


FIG. 4. The geometry and loading of two three-layered two-dimensional functionally graded beam configurations.

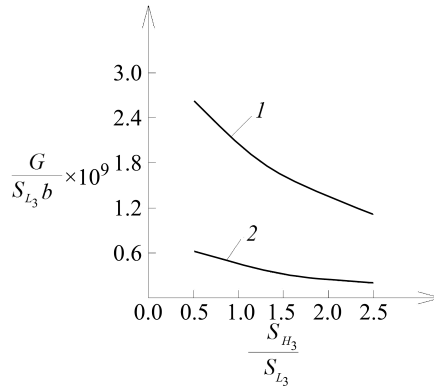


FIG. 5. Variation of the strain energy release rate in non-dimensional form with  $S_{H_3}/S_{L_3}$  ratio (curve 1 – for the three-layered beam configuration with a delamination crack between layers 2 and 3 (refer to Fig. 4a), curve 2 – for the three-layered beam configuration with a delamination crack between layers 1 and 2 (refer to Fig. 4b)).

is plotted against  $S_{B_3}/S_{L_3}$  ratio in Fig. 6 at  $S_{H_3}/S_{L_3} = 1.6$ . The curves in Fig. 6 indicate that the strain energy release rate decreases with increasing of  $S_{B_3}/S_{L_3}$  ratio. The influence of non-linear behaviour of the material on the delamination fracture is also investigated. For this purpose, the strain energy release rate derived assuming linear-elastic behaviour of the functionally graded beam configuration shown in Fig. 4a is plotted in non-dimensional form against  $S_{B_3}/S_{L_3}$  ratio in Fig. 6 for comparison with the non-linear solution. It should be noted that the linear-elastic solution is derived by substituting of  $m_i = 1$  in formula (2.16). It can be concluded from Fig. 6 that the non-linear behaviour of material leads to increase of the strain energy release rate.

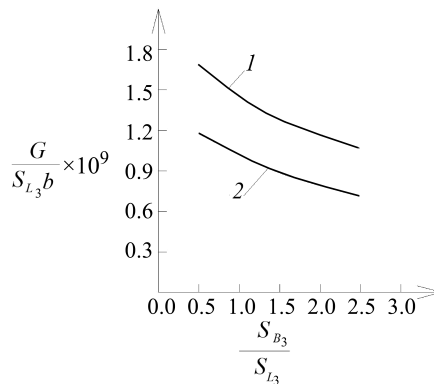


FIG. 6. Variation of the strain energy release rate in non-dimensional form with  $S_{B_3}/S_{L_3}$  ratio (curve 1 – at non-linear behaviour of the material, curve 2 – at linear-elastic behaviour of the material).

The distribution of the  $J$ -integral value along the delamination crack front is also studied. For this purpose, calculations of the  $J$ -integral value are carried-out by applying formula (2.24). The  $J$ -integral value is presented in non-dimensional form by using the formula  $J_N = J / (S_{L_3}b)$ . The three-layered beam configuration shown in Fig. 4a is analysed. Two patterns of material gradient are considered in order to evaluate the effect of material gradient along the width of layers on the distribution of the  $J$ -integral value. Pattern 1 is characterized by  $S_{L_1}/S_{L_3} = 1.2$ ,  $S_{H_1}/S_{L_1} = 1.1$ ,  $S_{B_1}/S_{L_1} = 1.3$ ,  $S_{L_2}/S_{L_3} = 1.5$ ,  $S_{H_2}/S_{L_2} = 1.1$ ,  $S_{B_2}/S_{L_2} = 1.2$ ,  $S_{H_3}/S_{L_3} = 1.1$  and  $S_{B_3}/S_{L_3} = 1.3$ . Pattern 2 of material gradient is characterized by  $S_{L_1}/S_{L_3} = 1.2$ ,  $S_{H_1}/S_{L_1} = -0.4$ ,  $S_{B_1}/S_{L_1} = 1.3$ ,  $S_{L_2}/S_{L_3} = 1.5$ ,  $S_{H_2}/S_{L_2} = -0.4$ ,  $S_{B_2}/S_{L_2} = 1.2$ ,  $S_{H_3}/S_{L_3} = -0.4$  and  $S_{B_3}/S_{L_3} = 1.3$ . The distribution of the  $J$ -integral value in non-dimensional form along the delamination crack front is presented in Fig. 7 at the two patterns of material gradient. Only the right-hand half of the delamination crack front is shown due to the symmetry. The horizontal axis is defined such that  $y_1/b = 0.0$  is in the delamination crack front centre. Thus,  $y_1/b = 0.5$  is in the right-hand lateral surface of the beam. One can observe in Fig. 7 that the  $J$ -integral value in the delamination crack front centre is the same for both patterns of material gradient. This is due to fact that the material property,  $S_i$ , does not depend on  $S_{H_i}$  at  $y_1 = 0$  (refer to formula (2.4)). Figure 7 shows that at pattern 1 of material gradient, the  $J$ -integral value has maximum in the delamination crack front centre and gradually decreases towards the beam lateral surface. This is due to the stiffness enhancement towards the beam lateral surfaces at  $S_{H_i}/S_{L_i} = 1.1$ ,  $i = 1, 2, 3$ . It can also be observed in Fig. 7 that at pattern 2 of material gradient, the distribution of the  $J$ -integral value is characterized by minimum in the delamination crack front centre and a gradual increase towards the beam lateral surface.

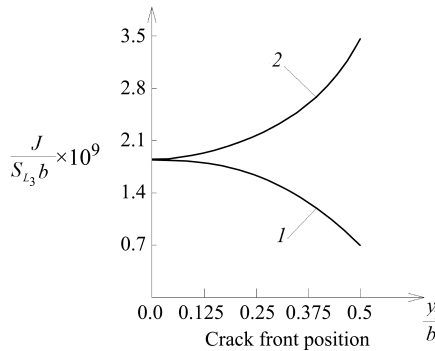


FIG. 7. Distribution of the  $J$ -integral value in non-dimensional form along the delamination crack front (curve 1 – at pattern 1 of material gradient, curve 2 – at pattern 2 of material gradient).

#### 4. CONCLUSIONS

The delamination fracture behaviour of a two-dimensional functionally graded multilayered beam configuration that exhibits material non-linearity is studied analytically. The beam under consideration is made of an arbitrary number of horizontal layers. A delamination crack is located arbitrary along the height of the beam cross-section. Each layer has individual thickness and material properties. Besides, the material is two-dimensional functionally graded in the cross-section of each layer. The fracture is studied in terms of the strain energy release rate by analysing the beam complementary strain energy. In order to verify the solution derived, the delamination crack is analysed also by using the  $J$ -integral approach. Parametric investigations are carried-out in order to evaluate the effects of material gradient, crack location and material non-linearity on the delamination fracture. The material gradient along the thickness and the width of layer is characterized by  $S_{B_i}/S_{L_i}$  and  $S_{H_i}/S_{L_i}$  ratios, respectively. The basic findings from the analysis developed in the present paper can be summarized as follows:

- 1) The strain energy release rate decreases with increasing of  $S_{B_i}/S_{L_i}$  and  $S_{H_i}/S_{L_i}$  ratios.
- 2) The strain energy release rate decreases with increasing of the lower crack arm thickness (the upper crack arm is free of stresses).
- 3) The non-linear behaviour of the material leads to increase of the strain energy release rate.
- 4) The distribution of the  $J$ -integral value along the delamination crack front is greatly affected by the material gradient along the width of the layers.
- 5) The delamination fracture in two-dimensional functionally graded multilayered beams with non-linear behaviour of material can be optimized by choosing suitable material gradients.

#### REFERENCES

1. BOHIDAR S.K., SHARMA R., MISHRA P.R., *Functionally graded materials: A critical review*, International Journal of Research, **1**(7): 289–301, 2014.
2. TILBROOK M.T., MOON R.J., HOFFMAN M., *Crack propagation in graded composites*, Composite Science and Technology, **65**(2): 201–220, 2005.
3. UPADHYAY A.K., SIMHA K.R.Y., *Equivalent homogeneous variable depth beams for cracked FGM beams; compliance approach*, International Journal of Fracture, **144**(3): 209–213, 2007.
4. PANIGRAHI B., POHIT G., *Nonlinear modelling and dynamic analysis of cracked Timoshenko functionally graded beams based on neutral surface approach*, Proceedings of the

Institution of Mechanical Engineers, Part C: Journal of Mechanical Engineering Science, **230**(9): 1468–1497, 2016.

5. RIZOV V.I., *Analytical study of elastic-plastic longitudinal fracture in a functionally graded beam*, Strength, Fracture and Complexity, **10**(1): 11–22, 2017.
6. RIZOV V.I., *Delamination fracture in a functionally graded multilayered beam with material nonlinearity*, Archive of Applied Mechanics, **87**(6): 1037–1048, 2017.
7. SZEKRENYES A., *Nonsingular crack modelling in orthotropic plates by four equivalent single layers*, European Journal of Mechanics – A/Solids, **55**: 73–99, 2016.
8. HSUEH C.H., TUAN W.H., WEI W.C.J., *Analyses of steady-state interface fracture of elastic multilayered beams under four-point bending*, Scripta Materialia, **60**(8): 721–724, 2009.
9. LUBLINER J., *Plasticity theory* (Rev. Ed.), University of California, Berkeley, CA, 2006.
10. PETROV V.V., *Non-linear incremental structural mechanics*, Infra-Injeneria, M., 2014.
11. HUTCHINSON J.W., SUO Z., *Mixed mode cracking in layered materials*, Advances in Applied Mechanics, **29**: 63–191, 1991.
12. BROEK D., *Elementary engineering fracture mechanics*, Springer, 1986.

*Received August 11, 2017; accepted version December 19, 2017.*

---